

Dynamical Mass of the Young Brown Dwarf Companion PZ Tel B

KYLE FRANSON ^{1,*} AND BRENDAN P. BOWLER ¹

¹*Department of Astronomy, The University of Texas at Austin, Austin, TX 78712, USA*

ABSTRACT

Dynamical masses of giant planets and brown dwarfs are critical tools for empirically validating substellar evolutionary models and their underlying assumptions. We present a measurement of the dynamical mass and an updated orbit of PZ Tel B, a young brown dwarf companion orbiting a late-G member of the β Pic moving group. PZ Tel A exhibits an astrometric acceleration between Hipparcos and Gaia EDR3, which enables the direct determination of the companion’s mass. We have also acquired new Keck/NIRC2 adaptive optics imaging of the system, which increases the total baseline of relative astrometry to 15 years. Our joint orbit fit yields a dynamical mass of $27_{-9}^{+25} M_{\text{Jup}}$, semi-major axis of 27_{-4}^{+14} au, eccentricity of $0.52_{-0.10}^{+0.08}$, and inclination of $91.73_{-0.32}^{+0.36^\circ}$. The companion’s mass is consistent within 1.1σ of predictions from four grids of hot-start evolutionary models. The joint orbit fit also indicates a more modest eccentricity of PZ Tel B than previous results. PZ Tel joins a small number of young (<200 Myr) systems with benchmark substellar companions that have dynamical masses and precise ages from moving group membership.

Keywords: Brown dwarfs (185) — Direct imaging (387) — Astrometry (80) — Orbit determination (1175)

1. INTRODUCTION

Model-independent dynamical masses of giant planets and brown dwarfs offer unique probes into the formation and evolution of substellar objects. When paired with a bolometric luminosity and age constraint, these objects facilitate precision tests of substellar cooling models and their underlying assumptions about the initial entropy, atmospheric physics, and internal structure of low-temperature objects. These benchmark systems are rare, largely owing to the low intrinsic rate of substellar companions within a few tens to hundreds of au. The Gemini Planet Imager Exoplanet Survey measured an occurrence rate of $0.8_{-0.5}^{+0.8}\%$ for brown dwarf companions ($13\text{--}80 M_{\text{Jup}}$) around all stars ($0.2\text{--}5 M_{\odot}$) at semi-major axes from $10\text{--}100$ au. (Nielsen et al. 2019). The SpHERE INfrared Exoplanet survey measured a slightly higher occurrence rate of $5.8_{-2.8}^{+4.7}\%$ for substellar companions ($1\text{--}75 M_{\text{Jup}}$) from $5\text{--}300$ au around FGK stars (Vigan et al. 2021). These are comparable to earlier studies that found brown dwarf companion frequencies of $\approx 1\text{--}4\%$ across all separations (e.g., Metchev & Hillen-

brand 2009; Brandt et al. 2014; Lafrenière et al. 2014; see Bowler & Nielsen 2018 and references therein).

The sample of substellar companions with dynamical masses and age constraints now amounts to ≈ 20 brown dwarf companions (e.g., Bowler et al. 2018; Cheetham et al. 2018; Brandt et al. 2019, 2020, 2021c; Kuzuhara et al. 2022; Bonavita et al. 2022; Franson et al. 2022, 2023a; Li et al. 2023) and giant planets (Dupuy et al. 2019; Lagrange et al. 2019; Nowak et al. 2020; Brandt et al. 2021a; Hinkley et al. 2022; Mesa et al. 2023; De Rosa et al. 2023; Franson et al. 2023b). Most of these benchmark companions orbit old field stars (>1 Gyr); only three planets— β Pic b, β Pic c, and AF Lep b—are young (<200 Myr) and have precise ages based on membership in kinematic associations (Dupuy et al. 2019; Nowak et al. 2020; Brandt et al. 2021a; Franson et al.

* NSF Graduate Research Fellow

2023b; De Rosa et al. 2023; Mesa et al. 2023).¹ Age-dating individual field stars is notoriously challenging, which can limit the precision of model tests for benchmark companions around young field stars (see e.g., HD 984 B; Franson et al. 2022) compared to objects in young moving groups.

The β Pictoris moving group (Barrado y Navascués et al. 1999; Zuckerman et al. 2001) is one of the best-studied nearby young kinematic associations. With around 150 bona-fide members and hundreds of additional candidates (e.g., Moór et al. 2013; Shkolnik et al. 2017; Gagné et al. 2018), this association has served as a laboratory for studying young debris disks (e.g., Kalas & Jewitt 1995; Kalas et al. 2004; Moór et al. 2020; Hinkley et al. 2021), giant planets (e.g., Lagrange et al. 2010; Liu et al. 2013; Macintosh et al. 2015; Dupuy et al. 2018; Plavchan et al. 2020; Nowak et al. 2020; Franson et al. 2023b), and brown dwarfs (e.g., Biller et al. 2010; Mugrauer et al. 2010; Schneider et al. 2017; Phillips et al. 2020a). The group spans a distance of $\sim 20\text{--}50$ pc (Gagné & Faherty 2018) and has an age of 24 ± 3 Myr (Bell et al. 2015; see also Table 6 of Miret-Roig et al. 2020 for a compilation of age estimates).

PZ Telescopii (=PZ Tel, HD 174429, HIP 92680) is a bright ($V=8.3$ mag; Kiraga 2012) G9IV (Torres et al. 2006) star at a distance of 47.25 ± 0.05 pc (Gaia Collaboration et al. 2022). It is a well-established member of the β Pic moving group (Zuckerman et al. 2001; Shkolnik et al. 2017), with BANYAN Σ (Gagné et al. 2018) giving a 96.8% probability of membership based on its Gaia DR3 astrometry and radial velocity measurement of -3.6 ± 1.6 km s⁻¹ (Gaia Collaboration et al. 2022). A brown dwarf orbiting PZ Tel was independently discovered by Biller et al. (2010) and Mugrauer et al. (2010) with Near-Infrared Coronagraphic Imager (NICI; Gemini South) and NaCo (VLT) adaptive optics (AO) imaging, respectively, with a contrast of $\Delta H = 5.38 \pm 0.09$ mag. At the time of its discovery, PZ Tel B was located at a projected separation of ~ 350 mas (~ 16.5 au; Biller et al. 2010; Mugrauer et al. 2010), but has gradually moved outward to over 500 mas based on the latest reported astrometric measurement in Stolker

et al. (2020). Model-inferred masses in the literature range from about $8 M_{\text{Jup}}$ to $60 M_{\text{Jup}}$, but typically fall between $20\text{--}50 M_{\text{Jup}}$ (e.g., $36 \pm 6 M_{\text{Jup}}$, Biller et al. 2010; $24\text{--}40 M_{\text{Jup}}$, Mugrauer et al. 2012; $3.3\text{--}24 M_{\text{Jup}}$, Schmidt et al. 2014; $45_{-7}^{+9} M_{\text{Jup}}$ and $59_{-8}^{+13} M_{\text{Jup}}$, Maire et al. 2016). PZ Tel B has been imaged from 2007 to 2018 with NaCo (VLT), NICI (Gemini South), SINFONI (VLT), and SPHERE (VLT), and shows orbital motion indicating a highly eccentric ($e \gtrsim 0.6$) and nearly edge-on orbit (e.g., Mugrauer et al. 2012; Ginski et al. 2014; Maire et al. 2016; Bowler et al. 2020). PZ Tel A exhibits a significant² astrometric acceleration of 3.7 ± 0.8 m s⁻¹ yr⁻¹ between Hipparcos and Gaia EDR3 in the Hipparcos-Gaia Catalog of Accelerations (HGCA; Brandt 2021), which for the first time enables the measurement of the companion’s dynamical mass based on the astrometric reflex motion of the host star.

Here, we perform a joint orbit fit of PZ Tel B incorporating all published astrometry, radial velocities, and the HGCA astrometric acceleration. We also report new Keck/NIRC2 K_s -band imaging that expands the total baseline of astrometric observations to 15 years. Through our orbit fit, we determine the dynamical mass of PZ Tel B for the first time and compare it against the predictions of four hot-start substellar evolutionary models using the moving group age and bolometric luminosity of the companion. We conclude by examining the impact of additional epochs of astrometry on the dynamical mass precision.

2. KECK/NIRC2 ADAPTIVE OPTICS IMAGING

We observed the PZ Tel system with the NIRC2 camera at W.M. Keck Observatory on UT 2022 September 17. Images were taken in K_s band in field-tracking mode with the 600 mas Lyot coronagraph and natural guide star AO (Wizinowich 2013). We obtained a total of 10 frames, each consisting of a single coadd with an integration time of 10 s. Due to the southern declination of PZ Tel ($\delta \sim -50^\circ$), the observations were taken at an airmass of 2.95 (altitude of 19:6 at the time of the observation). The median FWHM of the companion PSFs in the sequence is 60 mas, which is similar to the Keck K_s diffraction limit of 54 mas.

After subtracting darks and flat-fielding the science frames, we remove cosmic rays and bad pixels using the L.A.Cosmic algorithm (van Dokkum 2001). We then correct for geometric distortions from the optics of the imaging system using the solution of Service et al. (2016) for the narrow-field mode of the NIRC2 camera. An example frame from the sequence is shown in Figure

¹ The dynamical mass of HR 8799 e has been measured (Brandt et al. 2021b), but the age of the host star is not precisely determined. Zuckerman et al. (2011) and Lee & Song (2019) have linked the system to the Columba and β Pic moving groups, while Faramaz et al. (2021) later found that HR 8799 is likely a young field star. The ages of the Columba and β Pic moving groups are 45_{-7}^{+11} Myr and 24 ± 3 Myr, respectively (Bell et al. 2015). Sepulveda & Bowler (2022) derived an independent age constraint of $10\text{--}23$ Myr through fitting isochrones to the mass and fundamental properties of the host star.

² $\chi^2 = 21.3$, which corresponds to 4.2σ for 2 degrees of freedom.

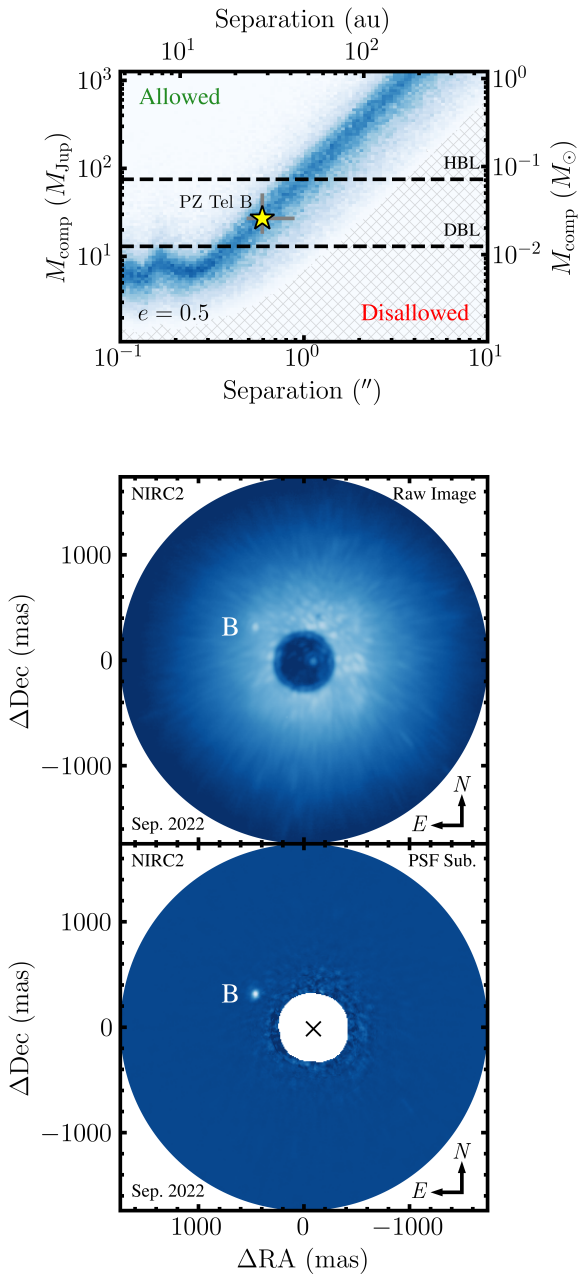


Figure 1. *Top:* Predicted mass of PZ Tel B as a function of projected separation based on its Hipparcos-Gaia astrometric acceleration. These predictions are generated following the procedure detailed in [Franson et al. \(2023a\)](#) except using an eccentricity of 0.5 for our synthetic orbits. The yellow star denotes the companion’s dynamical mass ($27_{-9}^{+25} M_{\text{Jup}}$) and semi-major axis (27_{-4}^{+14} au). *Bottom:* Keck/NIRC2 K_s -band coronagraphic imaging of PZ Tel at an airmass of 2.95. The host star is visible behind the partially transparent 600 mas-diameter coronagraph. The top frame shows an example raw image from the sequence, while the bottom frame shows a PSF-subtracted image. The images are aligned such that north is up and east is to the left.

1. The companion is visible in the raw coronagraphic frames without the aid of PSF subtraction, while the host star is visible behind the partially transparent coronagraph. We also show a PSF-subtracted image generated by applying the Locally Optimized Combination of Images (LOCI; [Lafrenière et al. 2007](#)) algorithm with a NIRC2 reference PSF library comprising >2000 registered coronagraphic frames. Since our observations were not taken with Angular Differential Imaging ([Marois et al. 2006](#)), or pupil-tracking mode, we use Reference Star Differential Imaging ([Lafrenière et al. 2009](#)) with 100 frames selected from the reference library following [Bowler et al. \(2015\)](#). We adopt $N_A = 300$, $N_\delta = 1.5$, $g = 1$, and $dr = 2$ for the LOCI parameters. The companion is masked in the reduction.

To measure the astrometry of PZ Tel B, we determine the centroid of the companion and the host star in each raw image, measure the separation (ρ) and position angle (θ), and then adopt the mean of those quantities from all frames. The separation values incorporate the NIRC2 plate scale of 9.971 ± 0.004 mas/pixel ([Service et al. 2016](#)). The position angle is determined from the raw images using the following equation for NIRC2 observations in fixed pupil tracking mode, which uses FITS header values to determine the orientation of celestial north:

$$\theta = \theta_{\text{raw}} + \text{ROTPOSN} - \text{INSTANGL} - \theta_{\text{north}}. \quad (1)$$

Here, θ_{raw} is the position angle measured from a given frame before north alignment, ROTPOSN is the instrument rotator position, INSTANGL is the NIRC2 instrumental position angle zero point of $0^\circ 7$, and θ_{north} is the angle required to align the detector columns to celestial north ($0^\circ 262 \pm 0^\circ 020$; [Service et al. 2016](#)). Following [Franson et al. \(2022\)](#), uncertainties are determined by adding in quadrature the standard deviation of the individual ρ and θ measurements, the error on the [Service et al. \(2016\)](#) distortion correction of $\sigma_d = 1$ mas, the plate scale uncertainty, and the uncertainty of the north alignment.

Due to the high airmass of 2.95 at the time of the observation, we correct our astrometry for differential atmospheric refraction (DAR). The impact of DAR on relative astrometry can be divided into monochromatic and chromatic contributions. The monochromatic effect originates from the difference in zenith angle between two sources and has the effect of compressing images along the zenith direction. The chromatic effect occurs due to different wavelengths of light experiencing different levels of refraction in the atmosphere. This causes astrophysical sources to appear to elongate along the zenith direction. Differences in spectral slope between

two sources can then alter their respective positions on the detector, influencing the astrometry measured from the ground.

For each image in the sequence, we compute the monochromatic DAR using Equation 12 of Gubler & Tytler (1998). The `refco` function from the Starlink AST C library (Berry et al. 2016) is used to calculate the refraction constants A and B given the relative humidity, temperature, and pressure measured at the Canada–France–Hawaii Telescope (CFHT) weather station³ at the time of the exposure and the NIRC2 K_s central wavelength of $2.146 \mu\text{m}$.⁴ For the zenith separation, we project the angular distance between PZ Tel A and B for each individual frame onto its zenith axis determined prior to DAR correction. The average zenith separation for our sequence is 235 mas and the average monochromatic DAR is 0.35 mas.

For the chromatic DAR, we use BT-Settl model spectra (Allard et al. 2012a,b) to compute the effective wavelength for each source through the K_s filter via the equation

$$\lambda_{\text{eff}} = \frac{\int \lambda I(\lambda) T(\lambda) d\lambda}{\int I(\lambda) T(\lambda) d\lambda}, \quad (2)$$

where $I(\lambda)$ is the model spectrum and $T(\lambda)$ is the filter transmission profile. For the host star, we adopt a $T_{\text{eff}} = 5200 \text{ K}$ and $\log g = 4.0 \text{ dex}$ spectrum based on the effective temperature and surface gravity of PZ Tel A ($T_{\text{eff}} = 5173 \text{ K}$, $\log g = 4.16 \text{ dex}$; Luck 2018). For PZ Tel B, Maire et al. (2016) determined an effective temperature of $2700 \pm 100 \text{ K}$ and surface gravity $\log g < 4.5 \text{ dex}$. We thus adopt a model spectrum with $T_{\text{eff}} = 2700 \text{ K}$ and $\log g = 4.0 \text{ dex}$ for this purpose. `refco` is then used to compute refraction constants for both sources, given their K_s -band effective wavelengths and the CFHT weather parameters. Finally, we use Equation 11 of Gubler & Tytler (1998) to compute the chromatic DAR for each frame. The average chromatic DAR across the sequence is 1.54 mas. The amount of relative refraction for PZ Tel B is smaller than PZ Tel A. Since PZ Tel B is at a lower zenith angle (higher elevation) in our imaging, chromatic DAR reduces their apparent separation along the zenith axis. To correct our astrometry, we adjust the astrometry measured for each individual frame and increase the separation along the zenith angle by the sum of the two DAR compo-

nents for that image. Averaged across all frames, this produces a separation of $\rho = 636.1 \pm 1.7 \text{ mas}$ and position angle of $\theta = 59^\circ 33 \pm 0^\circ 10$. Correcting for DAR increases ρ by 0.7 mas and decreases θ by $0^\circ 16$.

The partially transparent coronagraph mask has been found to introduce additional systematic uncertainty on the host-star position (e.g., Konopacky et al. 2016). Bowler et al. (2018) found that the 600 mas mask imparts astrometric uncertainty at the 4–5 mas-level in separation based on the observed astrometric jitter of the brown dwarf companion Gl 758 B. This corresponds to $\pm 0^\circ 4$ – $0^\circ 5$ in position angle at the separation of PZ Tel B. This may impact our astrometry, so we conservatively adopt a noise floor of $\pm 5 \text{ mas}$ in separation and $\pm 0^\circ 5$ in position angle. Our final astrometry is then $\rho = 636 \pm 5 \text{ mas}$ and $\theta = 59^\circ 3 \pm 0^\circ 5$.

3. 3D ORBIT FIT

To measure the dynamical mass of PZ Tel B, we perform a joint orbit fit of all available relative astrometry, radial velocities (RVs), and the absolute astrometry from Hipparcos and Gaia EDR3 in the HGCA. The published relative astrometry of this system comprises 33 measurements from June 2007 to June 2018. This astrometry was previously assembled in Bowler et al. (2020), which included epochs from Biller et al. (2010), Mugrauer et al. (2012), Ginski et al. (2014), Beust et al. (2016), and Maire et al. (2016). We supplement the Bowler et al. (2020) compilation with three additional epochs from 2016 taken in the SHINE survey (Langlois et al. 2021), two measurements from May 2018 reported in Musso Barcucci et al. (2019), and two measurements from June 2018 reported in Stolker et al. (2020). We also include our new September 2022 Keck/NIRC2 astrometry in the orbit fit for a total of 34 data points.

Precise radial velocity measurements of PZ Tel A are obtained from the HARPS–RVBANK archive (Trifonov et al. 2020). They total 42 measurements taken between April 2009 and October 2017 with the High Accuracy Radial velocity Planet Searcher (HARPS; Pepe et al. 2002; Mayor et al. 2003), a high-resolution ($R \approx 115,000$) optical spectrograph mounted on the 3.6 m ESO telescope at La Silla Observatory. The RVs have an rms value of 513 m s^{-1} and a median uncertainty on each individual measurement of 4.2 m s^{-1} . The dominant sources of instrumental and astrophysical noise are likely stellar activity due to the star’s youth and broadening from its fast rotation ($v \sin i = 73 \pm 5 \text{ km s}^{-1}$; Jenkins et al. 2012). We use the measurements in the catalog under the “DRVmlcnzp” column, which incorporates correc-

³ The average relative humidity, temperature, and pressure during our observations of PZ Tel were 79.7%, 3.053°C, and 618.7 mb. The CFHT weather station archive can be found at <http://mkwc.ifa.hawaii.edu/archive/wx/cfht/>.

⁴ <http://www2.keck.hawaii.edu/inst/nirc2/filters.html>

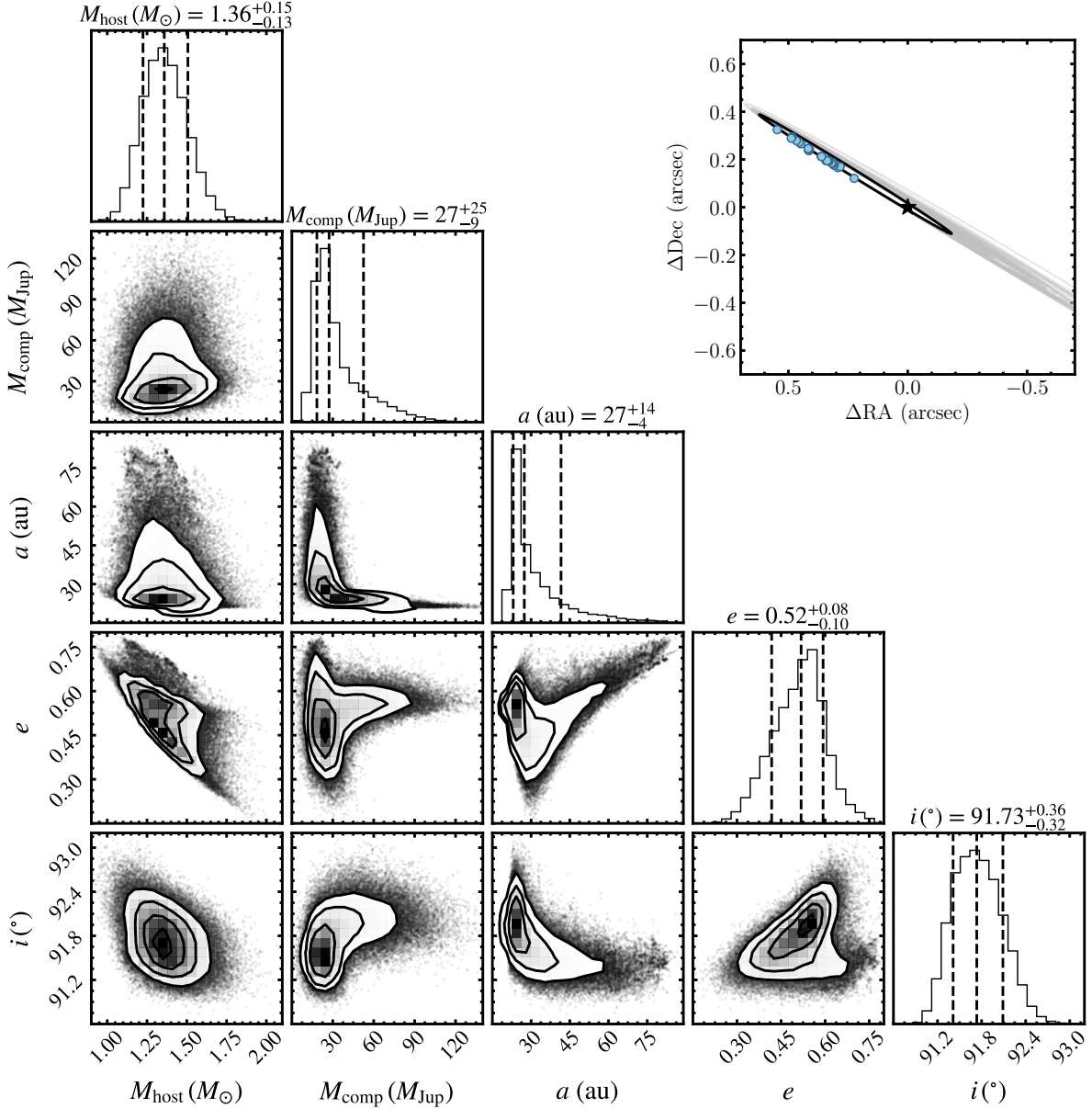


Figure 2. Joint posterior distributions for host-star mass (M_{host}), companion mass (M_{comp}), semi-major axis (a), eccentricity (e), and inclination (i) for the orbit fit of PZ Tel B. Diagonal panels show the marginalized distributions for each parameter. Off-diagonal panels show the covariance between orbital elements. The plot in the upper right shows the sky-projected orbit of PZ Tel B over time. The gray curves are drawn from the MCMC chains, while the black curve highlights the maximum-likelihood orbit. We measure a dynamical mass of $27^{+25}_{-9} M_{\text{Jup}}$ for PZ Tel B.

tions for nightly zero-point variations, intra-night RV drift, and a discontinuity in the absolute RV associated with the May 2015 upgrade of the HARPS fibers (Lo Curto et al. 2015).

Our joint orbit fit is carried out with the `orvara` orbit fitting package (Brandt et al. 2021d), which uses the parallel-tempered Markov chain Monte Carlo (PT-MCMC) ensemble sampler in `emcee` (Foreman-Mackey et al. 2013) to sample the orbit element posterior parameter space. `orvara` directly fits the following quan-

ties: the host star mass (M_{host}), the companion mass (M_{comp}), semi-major axis (a), inclination (i), longitude of ascending node (Ω), the longitude at the reference epoch of 2010.0 (λ_{ref}), and an RV jitter term (σ_{RV}). Eccentricity (e) and argument of periastron (ω) are parameterized as $\sqrt{e} \sin \omega$ and $\sqrt{e} \cos \omega$ in the fit to avoid the Lucy-Sweeney bias against circular orbits (Lucy & Sweeney 1971). `orvara` analytically marginalizes over the parallax, barycenter proper motion, and instrumental RV zero-points to increase computational efficiency.

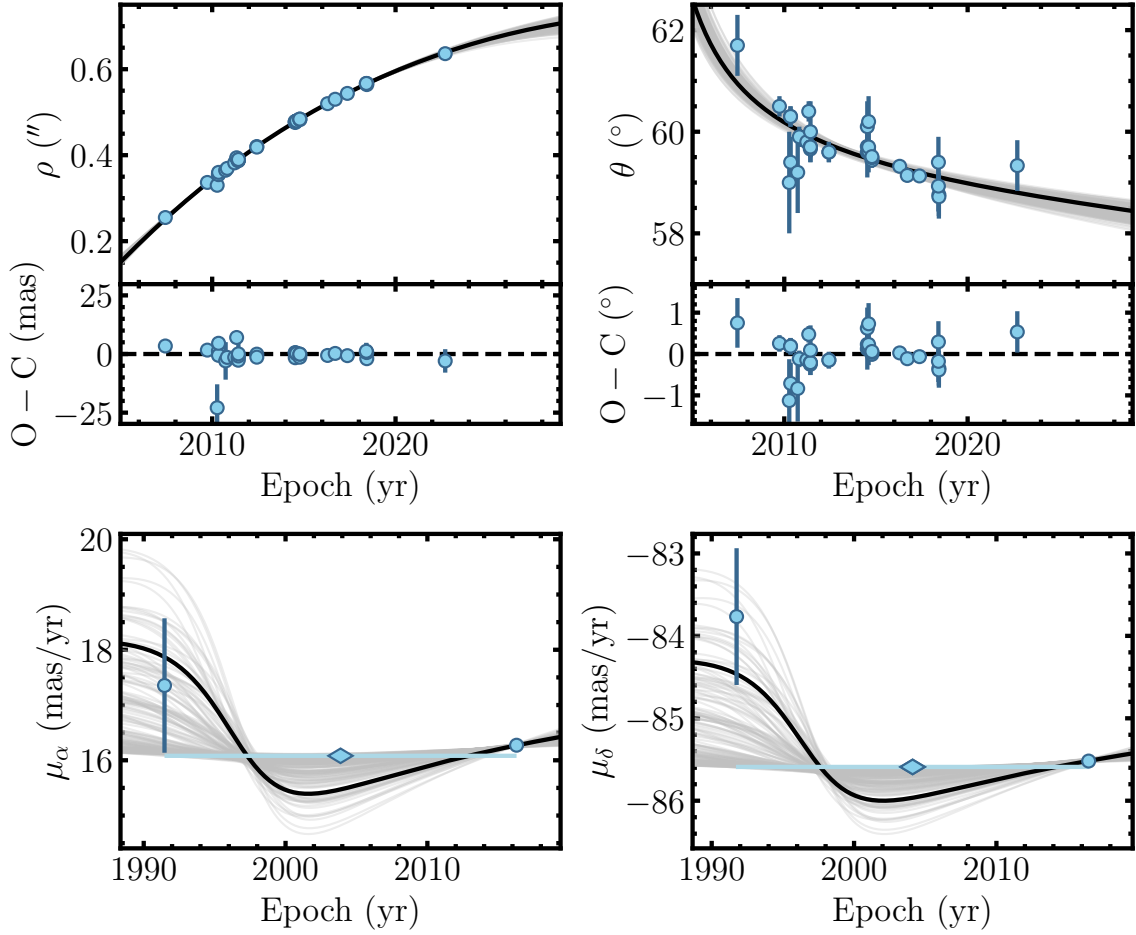


Figure 3. Comparison of relative and absolute astrometry against the PZ Tel B orbit fit. The upper plots show the separation (ρ) and position angle (θ) of PZ Tel B over time. The lower plots display the HGCA proper motions. Note that the middle point at ≈ 2004 is a joint proper motion that averages the astrometric reflex motion of PZ Tel A over the 25 yr time baseline between Hipparcos and Gaia EDR3. The gray curves are drawn from the MCMC chains, while the black curves highlight the maximum-likelihood orbit.

We adopt uninformative priors for all orbital elements and the companion mass. The host-star mass prior is assigned a Gaussian distribution of $1.1 \pm 0.2 M_{\odot}$ based on typical values for the mass of PZ Tel A in the literature (e.g., $1.25^{+0.05}_{-0.20} M_{\odot}$ from D’Antona & Mazzitelli 1994; $1.02 \pm 0.04 M_{\odot}$ from Allende Prieto & Lambert 1999, $1.2 \pm 0.1 M_{\odot}$ from Tetzlaff et al. 2011; $1.13 \pm 0.03 M_{\odot}$ from Jenkins et al. 2012; $1.14 M_{\odot}$ from Zúñiga-Fernández et al. 2021). The Gaia EDR3 value of 21.162 ± 0.022 mas (Gaia Collaboration et al. 2021) is used for the parallax prior. Our priors for all fitted orbit elements and physical parameters are shown in Table 1.

We use a total of 100 walkers, 20 temperatures, and 10^6 total steps to sample the parameter space. The posterior distribution for the parallel-tempered sampling algorithm is described by the coldest-temperature chain (see e.g., Vousden et al. 2016). We discard the first 50% (5000 steps of each walker) as burn-in. Table 1 shows

the marginalized parameter posteriors from the orbit fit. Figure 2 displays the posterior distributions for select orbital elements. A comparison of the relative astrometry of PZ Tel B and HGCA proper motions to a swarm of orbits drawn from the orbit fit is shown in Figure 3. We measure a dynamical mass of $27^{+25}_{-9} M_{\text{Jup}}$, semi-major axis of 27^{+14}_{-4} au, inclination of $91.73^{+0.36}_{-0.32} \circ$, and eccentricity of $0.52^{+0.08}_{-0.10}$. The orbital period is 120^{+110}_{-30} yr and the time of periastron is $T_0 = 1997.2^{+4.7}_{-1.8}$.

There is covariance between the companion mass and semi-major axis posteriors: the high-mass tail in companion mass occurs when semi-major axis is small, while the tail to large semi-major axes is restricted to low values of the dynamical mass. This is caused by the similarity of the Hipparcos-Gaia joint proper motion to the Gaia EDR3 proper motion in combination with the limited amount of position angle change over the relative astrometry baseline (see Figure 3). While the proper

Table 1. PZ Tel B Orbit Fit Results

Parameter	Median $\pm 1\sigma$	95.4% C.I.	Prior
Fitted Parameters			
$M_{\text{comp}} (M_{\text{Jup}})$	27_{-9}^{+25}	(12, 88)	$1/M_{\text{comp}}$ (log-flat)
$M_{\text{host}} (M_{\odot})$	$1.36_{-0.13}^{+0.15}$	(1.11, 1.67)	$1.1 \pm 0.2 M_{\odot}$ (Gaussian)
a (AU)	27_{-4}^{+14}	(22, 66)	$1/a$ (log-flat)
i ($^{\circ}$)	$91.73_{-0.32}^{+0.36}$	(91.17, 92.43)	$\sin(i)$, $0^{\circ} < i < 180^{\circ}$
$\sqrt{e} \sin \omega$	$0.2_{-0.8}^{+0.4}$	(-0.8, 0.8)	Uniform
$\sqrt{e} \cos \omega$	0.0 ± 0.6	(-0.7, 0.7)	Uniform
Ω ($^{\circ}$)	$238.62_{-0.23}^{+0.21} a$	(238.17, 238.99) ^a	Uniform
λ_{ref} ($^{\circ}$) ^b	110_{-40}^{+160}	(70, 290)	Uniform
Parallax (mas)	21.163 ± 0.031	(21.101, 21.224)	21.162 ± 0.022 mas (Gaussian)
μ_{α} (mas yr ⁻¹)	$16.63_{-0.12}^{+0.34}$	(16.41, 17.40)	Uniform
μ_{δ} (mas yr ⁻¹)	$-85.27_{-0.08}^{+0.21}$	(-85.42, -84.80)	Uniform
RV Jitter σ_{RV} (ms ⁻¹)	520_{-50}^{+60}	. . .	$1/\sigma_{\text{RV}}$ (log-flat), $\sigma_{\text{RV}} \in (0, 1000 \text{ms}^{-1}]$
Derived Parameters			
P (yr)	120_{-30}^{+110}	(80, 470)	. . .
e	$0.52_{-0.10}^{+0.08}$	(0.32, 0.69)	. . .
ω ($^{\circ}$)	$50_{-30}^{+50} c$	(10, 120) ^c	. . .
T_0 (JD)	2450500_{-700}^{+1700}	(2449200, 2454000)	. . .
T_0 (yr)	$1997.2_{-1.8}^{+4.7}$	(1993.7, 2006.7)	. . .
$q (= M_{\text{comp}}/M_{\text{host}})$	$0.019_{-0.006}^{+0.018}$	(0.009, 0.062)	. . .

^aThe posterior distribution for Ω consists of two distinct peaks separated by 180° . The values shown in the table correspond to the higher peak. The other peak is located at $58.61_{-0.22}^{+0.20}$ with a 95.4% confidence interval of (58.17, 58.97).

^bMean longitude at the reference epoch of 2010.0.

^cThe posterior distribution for ω is bimodal, with two peaks with similar shapes separated by 180° . The values shown in the table correspond to the slightly higher peak. The other peak is located at 220_{-20}^{+50} with a 95.4% confidence interval of (190, 290).

motions are significantly different at the 4σ -level, there remains a degeneracy between large-semi-major-axis solutions, where the proper motion change is small between Hipparcos and Gaia, and small-semi-major-axis solutions, in which the proper motion varies more substantially over the time baseline, but averages to the same value for the joint proper motion. Typically, this degeneracy would be broken by the relative astrometry. However, the small amount of position angle change limits the ability to distinguish these two solutions for PZ Tel B. The large-semi-major-axis orbits from the fit are only permitted if the companion mass is lower ($\lesssim 30 M_{\text{Jup}}$), since higher masses and longer orbital periods would cause more significant changes in the absolute astrometry that would not average to the value of the observed joint proper motion.

The orbit fit prefers higher values of the primary mass ($1.36_{-0.13}^{+0.15} M_{\odot}$) than our prior of $1.1 \pm 0.2 M_{\odot}$. To assess

the impact of this prior on the resultant orbit elements, we conduct orbit fits with a narrow ($1.1 \pm 0.1 M_{\odot}$) and a wide ($1.1 \pm 0.5 M_{\odot}$) prior on the host-star mass. For these fits, we use the same number of walkers, temperatures, and steps as our adopted orbit fit, and again discard the first 50% of each walker as burn-in. Both priors yield consistent orbit elements within the uncertainties. The narrow prior produces $M_{\text{comp}} = 25_{-8}^{+26} M_{\text{Jup}}$, $a = 28_{-4}^{+16}$ au, $e = 0.58_{-0.07}^{+0.06}$, and $i = 91.89_{-0.34}^{+0.35}$. The wide prior yields $M_{\text{comp}} = 34_{-12}^{+26} M_{\text{Jup}}$, $a = 25_{-3}^{+8}$ au, $e = 0.42_{-0.16}^{+0.10}$, and $i = 91.55_{-0.28}^{+0.32}$. We thus find that the choice of host-star mass prior has a small impact on our dynamical mass and orbit fit.

4. DISCUSSION

4.1. Mass of PZ Tel B

The dynamical mass of $27_{-9}^{+25} M_{\text{Jup}}$ is right-skewed, with a tail that extends to significantly higher masses.

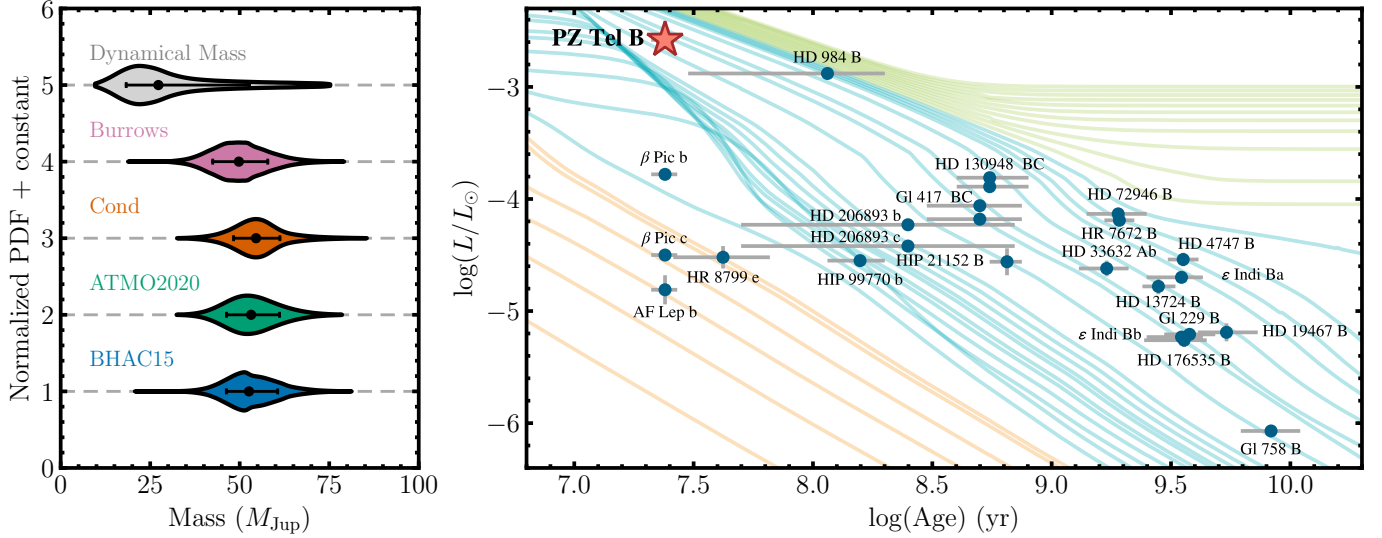


Figure 4. *Left:* Comparison of the dynamical mass of PZ Tel B with the predicted masses from four hot-start evolutionary models. The median and 68.3% confidence interval are highlighted for each distribution. The inferred masses are consistent with the dynamical mass to within 1σ . *Right:* Dynamical masses with well-constrained ages and luminosities. The background models show the luminosity evolution of planets (orange), brown dwarfs (blue) and low-mass stars (green) of a given mass from Burrows et al. (1997). PZ Tel B (highlighted in red) is among the few systems with a precise dynamical mass and a well-constrained age under 200 Myr. The luminosities and ages for the majority of systems are tabulated in Table 1 of Franson et al. (2022). We also include HD 206893 bc (Hinkley et al. 2022), HIP 21152 B (Bonavita et al. 2022; Kuzuhara et al. 2022; Franson et al. 2023a), ϵ Indi Bab (Chen et al. 2022), HIP 99770 b (Currie et al. 2022), HD 176535 B (Li et al. 2023), and AF Lep b (Franson et al. 2023b; Mesa et al. 2023; De Rosa et al. 2023). The age for HD 206893 bc is from Delorme et al. (2017) and luminosities of ϵ Indi Bab are from King et al. (2010). The luminosity from Franson et al. (2023b) is adopted for AF Lep b.

The hydrogen-burning limit (HBL), defined as the mass at which 50% of an object’s energy is generated via hydrogen fusion, marks the boundary between brown dwarfs and low-mass stars (Reid & Hawley 2005). The precise value can vary depending on assumptions about the equation of state, rotation, composition, and atmospheric properties (Burrows et al. 1997), but generally ranges from $70\text{--}80 M_{\text{Jup}}$ (e.g., Saumon & Marley 2008; Scudlaire et al. 2008; Baraffe et al. 2015; Dupuy & Liu 2017). Adopting $75 M_{\text{Jup}}$ as the substellar boundary, 95.0% of the dynamical mass posterior is below this value. At a lower HBL threshold $70 M_{\text{Jup}}$, 93.3% of the dynamical mass is below the value. Similar to the HBL, the deuterium-burning limit (DBL), which traditionally demarcates planets and brown dwarfs (Boss et al. 2003, 2007), can vary based on a given objects’ helium abundance, initial deuterium abundance, and metallicity, but generally is $\approx 13 M_{\text{Jup}}$ (Spiegel et al. 2011; Mollière & Mordasini 2012). A total of 96.5% of the dynamical mass posterior falls above $13 M_{\text{Jup}}$, while 91.5% lies between $13 M_{\text{Jup}}$ and $75 M_{\text{Jup}}$. We thus find that the dynamical mass of PZ Tel B is almost surely in the brown dwarf regime.

4.2. Orbit of PZ Tel B

Our orbit fit broadly recovers the high eccentricity long associated with PZ Tel B (e.g., Biller et al. 2010; Mugrauer et al. 2012), although our eccentricity posterior of $0.52^{+0.08}_{-0.10}$ is significantly lower than many previous determinations. Bowler et al. (2020) and Beust et al. (2016) found a higher eccentricity values of $0.89^{+0.10}_{-0.05}$ and $e > 0.91$, respectively, which were consistent with previous bounds of $e > 0.6$ from Biller et al. (2010), $0.66 \leq e \leq 0.99$ from Ginski et al. (2014), and $e \gtrsim 0.62$ from Maire et al. (2016). Our eccentricity is most similar to Musso Barucci et al. (2019), who found the eccentricity distribution to be multi-modal with a larger peak at $e \sim 0.55$ and smaller peak at $e \sim 1$. Note that the orbit fit from Musso Barucci et al. (2019) has the longest baseline of relative astrometry (2007–2018) among the fits in the literature. The semi-major axis of 27^{+14}_{-4} au that we find is compatible with previous orbit fits (e.g., $a \approx 31.3$ au, Musso Barucci et al. 2019; $a = 24.8^{+5.3}_{-5.5}$ au, Bowler et al. 2020; $a \gtrsim 24.5$ au, Maire et al. 2016).

The inclination from our orbit fit of $91.73^{+0.36}_{-0.32}$ is consistent with the results of previous fits which identified the companion as having an edge-on orbit (e.g., $i \sim 91.6^\circ$, Musso Barucci et al. 2019; $i = 93.4^{+1.2}_{-1.7}$, Bowler et al. 2020; $91^\circ < i < 96.1^\circ$, Maire et al. 2016). Bowler et al. (2023) determined the inclination of PZ Tel

A to be $i_* = 78.9_{-4.7}^{+11.0}^\circ$. This is compatible with alignment between the host star’s rotational axis and PZ Tel B’s orbit, given our measurement for the companion’s orbital inclination. Note, though, that misalignment remains a possibility. To conclusively determine the mutual alignment between the orbit of PZ Tel B and the rotation of its host star, one must determine the orientation of PZ Tel A’s rotation axis on the sky-plane (see e.g., Kraus et al. 2020).

4.3. Comparison with Evolutionary Model Predictions

Here, we compare the dynamical mass of PZ Tel B with the predicted masses from substellar evolutionary models that cover the age and luminosity of the companion. We consider four hot-start evolutionary models: the Burrows et al. (1997) grid, Cond (Baraffe et al. 2003), ATMO-2020 (Phillips et al. 2020b), and BHAC-15 (Baraffe et al. 2015).⁵

Our approach is to compute inferred masses for each evolutionary model given the age and luminosity of the companion. For the companion age, we adopt the age of the β Pic moving group of 24 ± 3 Myr from Bell et al. (2015). We compute the bolometric luminosity by applying a J -band bolometric correction of $BC_{J_{2\text{MASS}}} = 2.06 \pm 0.05$ mag⁶ from Herczeg & Hillenbrand (2015) based on the $M7 \pm 1$ spectral type of PZ Tel B (Maire et al. 2016). Liu et al. (2016) measured J -band photometry in the Mauna-Kea Observatories (MKO) system of 12.47 ± 0.20 mag, which corresponds to $J_{2\text{MASS}} = 12.52 \pm 0.20$ mag. With the Gaia DR3 parallax of 21.1621 ± 0.0223 mas (Gaia Collaboration et al. 2022), the absolute magnitude of PZ Tel B $M_{J_{2\text{MASS}}} = 9.15 \pm 0.20$ mag, which yields a bolometric luminosity of -2.59 ± 0.08 dex. This is consistent with the bolometric luminosity of -2.51 ± 0.10 dex determined in Maire et al. (2016) using K_s photometry and the K -band bolometric correction from Liu et al. (2010). We adopt our new bolometric luminosity value for the model comparison.

To generate inferred masses for each evolutionary model, we employ a Monte Carlo approach by randomly sampling from the bolometric luminosity and age distributions. The model grid is then linearly interpolated to determine the companion mass that corresponds to the specific age and luminosity value. This process is then repeated 10^6 times to build up a model-

inferred mass distribution. Figure 4 shows the inferred masses for the four grids we consider alongside the dynamical mass of PZ Tel B. To quantify the level of agreement between the dynamical mass and inferred masses, we follow Franson et al. (2023a) in determining $P(M_{\text{Inferred}} > M_{\text{Dynamical}})$, the probability that the inferred mass distribution function is greater than the dynamical mass distribution. Probabilities of $\approx 50\%$ signify that the two distributions are consistent with one another, while values near 0% or 100% correspond to the inferred mass being lower or higher than the dynamical mass, respectively. $P(M_{\text{Inferred}} > M_{\text{Dynamical}})$ can also be converted to a one-sided Gaussian-equivalent standard deviation, σ , via the equation

$$\sigma = \sqrt{2} \operatorname{erf}^{-1}(1 - 2P(M_{\text{Inferred}} > M_{\text{Dynamical}})). \quad (3)$$

For Burrows et al. (1997), $P(M_{\text{Inferred}} > M_{\text{Dynamical}}) = 82.0\%$, which corresponds to $+0.9\sigma$. For Cond, $P(M_{\text{Inferred}} > M_{\text{Dynamical}}) = 85.4\%$ ($+1.1\sigma$). For BHAC-15, $P(M_{\text{Inferred}} > M_{\text{Dynamical}}) = 84.4\%$ ($+1.0\sigma$). Finally, for ATMO-2020, $P(M_{\text{Inferred}} > M_{\text{Dynamical}}) = 84.6\%$ ($+1.0\sigma$). Overall, we find that all models are consistent with our dynamical mass to within about 1σ .

4.4. Improving the Dynamical Mass Precision

Finally, we explore the prospects for improving the precision of the dynamical mass of PZ Tel B with additional epochs of astrometric orbit monitoring. Our approach is to conduct orbit fits with mock astrometry at typical astrometric precisions of extreme AO (e.g., SPHERE, Beuzit et al. 2019; SCEXAO, Jovanovic et al. 2015, GPI, Macintosh et al. 2014) and GRAVITY (GRAVITY Collaboration et al. 2017) and examine how the dynamical mass posterior changes over time. For the extreme AO case, we adopt an uncertainty of ± 1.5 mas in separation and $\pm 0^\circ.2$ in position angle (e.g., Maire et al. 2016; Johnson-Groh et al. 2017). For GRAVITY astrometry, a typical positional uncertainty of ± 0.1 mas (e.g., Nowak et al. 2020; Hinkley et al. 2022) corresponds to an uncertainty of ± 0.1 mas in separation and $\pm 0^\circ.01$ in position angle.

Starting at $t = 2023.710$ (one year after our new Keck/NIRC2 epoch), we add new epochs of relative astrometry at a cadence of one mock observation per year. The separation and position angle for a given mock epoch are taken from the highest-likelihood orbit from our joint orbit fit with M_{comp} , a , and e all within $1 M_{\text{Jup}}$, 1 au, and 0.05 of their mean values in their respective posterior distributions. For each epoch, a new joint orbit fit with `orvara` is performed incorporating all of the previous epochs of mock relative astrometry alongside the true astrometry, radial velocities, and

⁵ Note that the Saumon & Marley (2008) models do not extend to objects as luminous as PZ Tel B.

⁶ Herczeg & Hillenbrand (2015) give a general uncertainty range on their bolometric corrections of 0.02–0.05 mag. For this analysis, we conservatively adopt the upper value for the uncertainty.

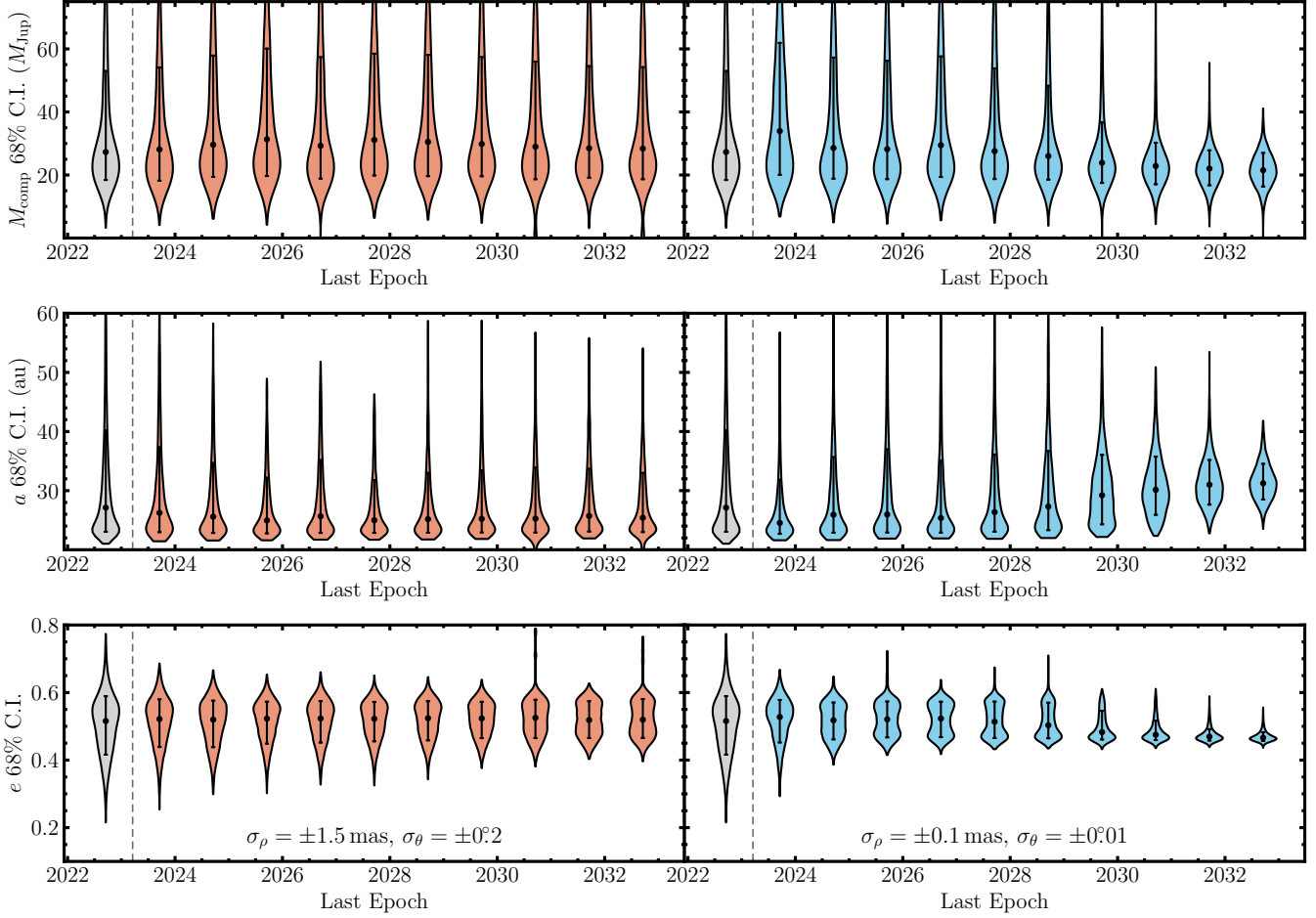


Figure 5. Companion mass (top), semi-major axis (middle), and eccentricity (bottom) posteriors from orbit fits with additional epochs of mock relative astrometry. The left panels (red distributions) show runs with additional epochs of 1.5 mas-precision astrometry (e.g., SPHERE, SCEXAO, GPI), while the right panels (blue distributions) display mock runs with additional epochs of 0.1 mas-precision astrometry (e.g., GRAVITY). The mock astrometry is added with a 1-year cadence; each distribution shows an orbit fit with annual epochs from 2023.77 to its last epoch. The posteriors from our orbit fit with no mock data are shown in gray. The median and 68.3% confidence interval are highlighted for each distribution.

HGCA proper motions of the system. For these orbit fits, we use 20 temperatures, 100 walkers, and 10^5 total steps. We discard the first 50% of each chain as burn-in.

Figure 5 shows the dynamical mass, semi-major axis, and eccentricity posteriors from our mock orbit fits. We find that at extreme-AO-level precisions, the constraints on companion mass, semi-major axis, and eccentricity are not meaningfully improved with additional astrometry over this ten-year timeframe. At GRAVITY-level precisions, these constraints can be substantially improved with continued astrometric monitoring. After ≈ 8 years of annual GRAVITY measurements, this exercise predicts that the dynamical mass would be constrained to the $\pm 5 M_{\text{Jup}}$ level, the semi-major axis would be constrained to the ± 5 au level, and the eccentricity would be constrained to ± 0.03 . The 68% credible interval for the companion mass decreases from $34 M_{\text{Jup}}$ to $11 M_{\text{Jup}}$

between our orbit fit with no mock data and an orbit fit with ten epochs of additional GRAVITY astrometry. The credible intervals for the semi-major axis and eccentricity decrease from 18 au to 6 au and 0.18 to 0.03, respectively.

There are several aspects of the PZ Tel system that create challenges for improving the mass constraint. The companion is currently approaching apastron, where the separation changes the least year-over-year. Furthermore, the nearly edge-on orbit means that the annual change in position angle is small. The host star’s fast projected rotation ($v \sin i = 73 \pm 5 \text{ km s}^{-1}$; Jenkins et al. 2012) and youth make the detection of an RV acceleration challenging. Despite these challenges, astrometric monitoring with GRAVITY is capable of significantly increasing the dynamical mass precision in the near future. Additional avenues for improving the mass con-

straint include measuring the RV of PZ Tel B with the Keck Planet Imager and Characterizer (e.g., Wang et al. 2021) and future Gaia monitoring of the host star.

5. SUMMARY

In this work, we measured the dynamical mass and orbit of the young brown dwarf companion PZ Tel B by combining Hipparcos-Gaia proper motions, relative astrometry including new Keck/NIRC2 imaging, and archival HARPS RVs. Our joint orbit fit produces a dynamical mass of $27_{-9}^{+25} M_{\text{Jup}}$, semi-major axis of 27_{-4}^{+14} au, eccentricity of $0.52_{-0.10}^{+0.08}$, and inclination of $91.73_{-0.32}^{+0.36} \circ$. The model-independent mass is consistent within 1.1σ of predicted masses from hot-start evolutionary models given the companion’s age and luminosity. The eccentricity from our fit is significantly lower than many previous orbit fits, which generally identified eccentricities above 0.6. We also examined the impact of additional epochs of relative astrometry on the precision of the dynamical mass. High-precision astrometric monitoring with GRAVITY is capable of improving the mass constraint by a factor of three over ten epochs. PZ Tel B joins β Pic b, β Pic c, and AF Lep b as the only substellar companions in young associations with dynamical masses.

6. ACKNOWLEDGEMENTS

K.F. acknowledges support from the National Science Foundation Graduate Research Fellowship Program under Grant No. DGE-1610403. B.P.B. acknowledges support from the National Science Foundation grant AST-1909209, NASA Exoplanet Research Program grant 20-

XRP20.2-0119, and the Alfred P. Sloan Foundation. This work was supported by a NASA Keck PI Data Award, administered by the NASA Exoplanet Science Institute.

This work has made use of data from the European Space Agency (ESA) space mission Gaia. Gaia data are being processed by the Gaia Data Processing and Analysis Consortium (DPAC). Funding for the DPAC is provided by national institutions, in particular the institutions participating in the Gaia Multi-Lateral Agreement (MLA). The Gaia mission website is <https://www.cosmos.esa.int/gaia>. The Gaia archive website is <https://archives.esac.esa.int/gaia>. This research has made use of the SIMBAD database and the VizieR catalogue access tool, CDS, Strasbourg, France. The Starlink software (Currie et al. 2014) is currently supported by the East Asian Observatory.

The authors wish to recognize and acknowledge the very significant cultural role and reverence that the summit of Maunakea has always had within the indigenous Hawaiian community. We are most fortunate to have the opportunity to conduct observations from this mountain.

Facilities: Keck:II (NIRC2)

Software: VIP (Gomez Gonzalez et al. 2017), orvara (Brandt et al. 2021d), ccdproc (Craig et al. 2017), photutils (Bradley et al. 2019), astropy (Astropy Collaboration et al. 2013, 2018), pandas (McKinney 2010), matplotlib (Hunter 2007), numpy (Harris et al. 2020), scipy (Virtanen et al. 2020), emcee (Foreman-Mackey et al. 2013), corner (Foreman-Mackey 2016), Starlink (Currie et al. 2014), AST (Berry et al. 2016)

REFERENCES

- Allard, F., Homeier, D., & Freytag, B. 2012a, RSPTA, 370, 2765, doi: [10.1098/rsta.2011.0269](https://doi.org/10.1098/rsta.2011.0269)
- Allard, F., Homeier, D., Freytag, B., & Sharp, C. 2012b, EAS Publications Series, 57, 3, doi: [10.1051/eas/1257001](https://doi.org/10.1051/eas/1257001)
- Allende Prieto, C., & Lambert, D. L. 1999, A&A, 352, 555. <http://ascl.net/astro-ph/9911002>
- Astropy Collaboration, Robitaille, T. P., Tollerud, E. J., et al. 2013, A&A, 558, A33, doi: [10.1051/0004-6361/201322068](https://doi.org/10.1051/0004-6361/201322068)
- Astropy Collaboration, Price-Whelan, A. M., Sipőcz, B. M., et al. 2018, AJ, 156, 123, doi: [10.3847/1538-3881/aabc4f](https://doi.org/10.3847/1538-3881/aabc4f)
- Baraffe, I., Chabrier, G., Barman, T. S., Allard, F., & Hauschildt, P. H. 2003, A&A, 402, 701, doi: [10.1051/0004-6361:20030252](https://doi.org/10.1051/0004-6361:20030252)
- Baraffe, I., Homeier, D., Allard, F., & Chabrier, G. 2015, A&A, 577, A42, doi: [10.1051/0004-6361/201425481](https://doi.org/10.1051/0004-6361/201425481)
- Barrado y Navascués, D., Stauffer, J. R., Song, I., & Caillault, J. P. 1999, ApJ, 520, L123, doi: [10.1086/312162](https://doi.org/10.1086/312162)
- Bell, C. P. M., Mamajek, E. E., & Naylor, T. 2015, MNRAS, 454, 593, doi: [10.1093/mnras/stv1981](https://doi.org/10.1093/mnras/stv1981)
- Berry, D. S., Warren-Smith, R. F., & Jenness, T. 2016, A&C, 15, 33, doi: [10.1016/j.ascom.2016.02.003](https://doi.org/10.1016/j.ascom.2016.02.003)
- Beust, H., Bonnefoy, M., Maire, A.-L., et al. 2016, A&A, 587, A89, doi: [10.1051/0004-6361/201527388](https://doi.org/10.1051/0004-6361/201527388)
- Beuzit, J.-L., Vigan, A., Mouillet, D., et al. 2019, A&A, 631, A155, doi: [10.1051/0004-6361/201935251](https://doi.org/10.1051/0004-6361/201935251)
- Biller, B. A., Liu, M. C., Wahhaj, Z., et al. 2010, ApJ, 720, L82, doi: [10.1088/2041-8205/720/1/L82](https://doi.org/10.1088/2041-8205/720/1/L82)
- Bonavita, M., Fontanive, C., Gratton, R., et al. 2022, MNRAS, 513, 5588, doi: [10.1093/mnras/stac1250](https://doi.org/10.1093/mnras/stac1250)
- Boss, A. P., Basri, G., Kumar, S. S., et al. 2003, in Brown Dwarfs, ed. E. Martín, Vol. 211, 529

- Boss, A. P., Butler, R. P., Hubbard, W. B., et al. 2007, *IAUTA*, 26A, 183, doi: [10.1017/S1743921306004509](https://doi.org/10.1017/S1743921306004509)
- Bowler, B. P., Blunt, S. C., & Nielsen, E. L. 2020, *AJ*, 159, 63, doi: [10.3847/1538-3881/ab5b11](https://doi.org/10.3847/1538-3881/ab5b11)
- Bowler, B. P., & Nielsen, E. L. 2018, in *Handbook of Exoplanets*, ed. H. J. Deeg & J. A. Belmonte (Cham: Springer International Publishing), 1967–1983, doi: [10.1007/978-3-319-55333-7_155](https://doi.org/10.1007/978-3-319-55333-7_155)
- Bowler, B. P., Shkolnik, E. L., Liu, M. C., et al. 2015, *ApJ*, 806, 62, doi: [10.1088/0004-637X/806/1/62](https://doi.org/10.1088/0004-637X/806/1/62)
- Bowler, B. P., Dupuy, T. J., Endl, M., et al. 2018, *AJ*, 155, 159, doi: [10.3847/1538-3881/aab2a6](https://doi.org/10.3847/1538-3881/aab2a6)
- Bowler, B. P., Tran, Q. H., Zhang, Z., et al. 2023, *arXiv e-prints*, arXiv:2301.04692, doi: [10.48550/arXiv.2301.04692](https://doi.org/10.48550/arXiv.2301.04692)
- Bradley, L., Sipőcz, B., Robitaille, T., et al. 2019, *Astropy/Photutils: V0.7.2*, Zenodo, doi: [10.5281/zenodo.3568287](https://doi.org/10.5281/zenodo.3568287)
- Brandt, G. M., Brandt, T. D., Dupuy, T. J., Li, Y., & Michalik, D. 2021a, *AJ*, 161, 179, doi: [10.3847/1538-3881/abdc2e](https://doi.org/10.3847/1538-3881/abdc2e)
- Brandt, G. M., Brandt, T. D., Dupuy, T. J., Michalik, D., & Marleau, G.-D. 2021b, *ApL*, 915, L16, doi: [10.3847/2041-8213/ac0540](https://doi.org/10.3847/2041-8213/ac0540)
- Brandt, G. M., Dupuy, T. J., Li, Y., et al. 2021c, *AJ*, 102, 301, doi: [10.3847/1538-3881/ac273e](https://doi.org/10.3847/1538-3881/ac273e)
- Brandt, T. D. 2021, *ApJS*, 254, 42, doi: [10.3847/1538-4365/abf93c](https://doi.org/10.3847/1538-4365/abf93c)
- Brandt, T. D., Dupuy, T. J., & Bowler, B. P. 2019, *AJ*, 158, 140, doi: [10.3847/1538-3881/ab04a8](https://doi.org/10.3847/1538-3881/ab04a8)
- Brandt, T. D., Dupuy, T. J., Bowler, B. P., et al. 2020, *AJ*, 160, 196, doi: [10.3847/1538-3881/abb45e](https://doi.org/10.3847/1538-3881/abb45e)
- Brandt, T. D., Dupuy, T. J., Li, Y., et al. 2021d, *AJ*, 162, 186, doi: [10.3847/1538-3881/ac042e](https://doi.org/10.3847/1538-3881/ac042e)
- Brandt, T. D., McElwain, M. W., Turner, E. L., et al. 2014, *ApJ*, 794, 159, doi: [10.1088/0004-637X/794/2/159](https://doi.org/10.1088/0004-637X/794/2/159)
- Burrows, A., Marley, M., Hubbard, W. B., et al. 1997, *ApJ*, 491, 856, doi: [10.1086/305002](https://doi.org/10.1086/305002)
- Cheetham, A., Ségransan, D., Peretti, S., et al. 2018, *A&A*, 614, A16, doi: [10.1051/0004-6361/201630136](https://doi.org/10.1051/0004-6361/201630136)
- Chen, M., Li, Y., Brandt, T. D., et al. 2022, *AJ*, 163, 288, doi: [10.3847/1538-3881/ac66d2](https://doi.org/10.3847/1538-3881/ac66d2)
- Craig, M., Crawford, S., Seifert, M., et al. 2017, *Astropy/Ccdproc: V1.3.0.Post1*, Zenodo, doi: [10.5281/zenodo.1069648](https://doi.org/10.5281/zenodo.1069648)
- Currie, M. J., Berry, D. S., Jenness, T., et al. 2014, in *Astronomical Society of the Pacific Conference Series*, Vol. 485, *Astronomical Data Analysis Software and Systems XXIII*, ed. N. Manset & P. Forshay, 391
- Currie, T., Brandt, G. M., Brandt, T. D., et al. 2022, *Direct Imaging and Astrometric Discovery of a Superjovian Planet Orbiting an Accelerating Star*, doi: [10.48550/arXiv.2212.00034](https://doi.org/10.48550/arXiv.2212.00034)
- D’Antona, F., & Mazzitelli, I. 1994, *ApJS*, 90, 467, doi: [10.1086/191867](https://doi.org/10.1086/191867)
- De Rosa, R. J., Nielsen, E. L., Wahhaj, Z., et al. 2023, *Direct Imaging Discovery of a Super-Jovian around the Young Sun-like Star AF Leporis*, doi: [10.48550/arXiv.2302.06332](https://doi.org/10.48550/arXiv.2302.06332)
- Delorme, P., Schmidt, T., Bonnefoy, M., et al. 2017, *A&A*, 608, A79, doi: [10.1051/0004-6361/201731145](https://doi.org/10.1051/0004-6361/201731145)
- Dupuy, T. J., Brandt, T. D., Kratter, K. M., & Bowler, B. P. 2019, *ApJL*, 871, L4, doi: [10.3847/2041-8213/aafb31](https://doi.org/10.3847/2041-8213/aafb31)
- Dupuy, T. J., & Liu, M. C. 2017, *ApJS*, 231, 15, doi: [10.3847/1538-4365/aa5e4c](https://doi.org/10.3847/1538-4365/aa5e4c)
- Dupuy, T. J., Liu, M. C., Allers, K. N., et al. 2018, *AJ*, 156, 57, doi: [10.3847/1538-3881/aacbc2](https://doi.org/10.3847/1538-3881/aacbc2)
- Faramaz, V., Marino, S., Booth, M., et al. 2021, *AJ*, 161, 271, doi: [10.3847/1538-3881/abf4e0](https://doi.org/10.3847/1538-3881/abf4e0)
- Foreman-Mackey, D. 2016, *JOSS*, 1, 24, doi: [10.21105/joss.00024](https://doi.org/10.21105/joss.00024)
- Foreman-Mackey, D., Hogg, D. W., Lang, D., & Goodman, J. 2013, *PASP*, 125, 306, doi: [10.1086/670067](https://doi.org/10.1086/670067)
- Franson, K., Bowler, B. P., Brandt, T. D., et al. 2022, *AJ*, 163, 50, doi: [10.3847/1538-3881/ac35e8](https://doi.org/10.3847/1538-3881/ac35e8)
- Franson, K., Bowler, B. P., Bonavita, M., et al. 2023a, *AJ*, 165, 39, doi: [10.3847/1538-3881/aca408](https://doi.org/10.3847/1538-3881/aca408)
- Franson, K., Bowler, B. P., Zhou, Y., et al. 2023b, *Astrometric Accelerations as Dynamical Beacons: A Giant Planet Imaged Inside the Debris Disk of the Young Star AF Lep*, doi: [10.48550/arXiv.2302.05420](https://doi.org/10.48550/arXiv.2302.05420)
- Gagné, J., & Faherty, J. K. 2018, *ApJ*, 862, 138, doi: [10.3847/1538-4357/aaca2e](https://doi.org/10.3847/1538-4357/aaca2e)
- Gagné, J., Mamajek, E. E., Malo, L., et al. 2018, *ApJ*, 856, 23, doi: [10.3847/1538-4357/aaae09](https://doi.org/10.3847/1538-4357/aaae09)
- Gaia Collaboration, Brown, A. G., Vallenari, A., Prusti, T., & de Bruijne, J. H. 2021, *A&A*, 650, C3, doi: [10.1051/0004-6361/202039657](https://doi.org/10.1051/0004-6361/202039657)
- Gaia Collaboration, Vallenari, A., Brown, A., Prusti, T., & et al. 2022, *A&A*, doi: [10.1051/0004-6361/202243940](https://doi.org/10.1051/0004-6361/202243940)
- Ginski, C., Schmidt, T. O. B., Mugrauer, M., et al. 2014, *MNRAS*, 444, 2280, doi: [10.1093/mnras/stu1586](https://doi.org/10.1093/mnras/stu1586)
- Gomez Gonzalez, C. A., Wertz, O., Absil, O., et al. 2017, *AJ*, 154, 7, doi: [10.3847/1538-3881/aa73d7](https://doi.org/10.3847/1538-3881/aa73d7)
- GRAVITY Collaboration, Abuter, R., Accardo, M., et al. 2017, *A&A*, 602, A94, doi: [10.1051/0004-6361/201730838](https://doi.org/10.1051/0004-6361/201730838)
- Gubler, J., & Tytler, D. 1998, *PASP*, 110, 738, doi: [10.1086/316172](https://doi.org/10.1086/316172)

- Harris, C. R., Millman, K. J., van der Walt, S. J., et al. 2020, *Natur*, 585, 357, doi: [10.1038/s41586-020-2649-2](https://doi.org/10.1038/s41586-020-2649-2)
- Herczeg, G. J., & Hillenbrand, L. A. 2015, *ApJ*, 808, 23, doi: [10.1088/0004-637X/808/1/23](https://doi.org/10.1088/0004-637X/808/1/23)
- Hinkley, S., Matthews, E. C., Lefevre, C., et al. 2021, *ApJ*, 912, 115, doi: [10.3847/1538-4357/abec6e](https://doi.org/10.3847/1538-4357/abec6e)
- Hinkley, S., Lacour, S., Marleau, G. D., et al. 2022, *A&A*, 671, L5, doi: [10.1051/0004-6361/202244727](https://doi.org/10.1051/0004-6361/202244727)
- Hunter, J. D. 2007, *CSE*, 9, 90, doi: [10.1109/MCSE.2007.55](https://doi.org/10.1109/MCSE.2007.55)
- Jenkins, J. S., Pavlenko, Y. V., Ivanyuk, O., et al. 2012, *MNRAS*, 420, 3587, doi: [10.1111/j.1365-2966.2011.20280.x](https://doi.org/10.1111/j.1365-2966.2011.20280.x)
- Johnson-Groh, M., Marois, C., De Rosa, R. J., et al. 2017, *AJ*, 153, 190, doi: [10.3847/1538-3881/aa6480](https://doi.org/10.3847/1538-3881/aa6480)
- Jovanovic, N., Martinache, F., Guyon, O., et al. 2015, *PASP*, 127, 890, doi: [10.1086/682989](https://doi.org/10.1086/682989)
- Kalas, P., & Jewitt, D. 1995, *AJ*, 110, 794, doi: [10.1086/117565](https://doi.org/10.1086/117565)
- Kalas, P., Liu, M. C., & Matthews, B. C. 2004, *Science*, 303, 1990, doi: [10.1126/science.1093420](https://doi.org/10.1126/science.1093420)
- King, R. R., McCaughrean, M. J., Homeier, D., et al. 2010, *A&A*, 510, A99, doi: [10.1051/0004-6361/200912981](https://doi.org/10.1051/0004-6361/200912981)
- Kiraga, M. 2012, *AcA*, 62, 67
- Konopacky, Q. M., Marois, C., Macintosh, B. A., et al. 2016, *AJ*, 152, 28, doi: [10.3847/0004-6256/152/2/28](https://doi.org/10.3847/0004-6256/152/2/28)
- Kraus, S., LeBouquin, J.-B., Kreplin, A., et al. 2020, *ApJL*, 897, L8, doi: [10.3847/2041-8213/ab9d27](https://doi.org/10.3847/2041-8213/ab9d27)
- Kuzuhara, M., Currie, T., Takarada, T., et al. 2022, *ApJL*, 934, L19, doi: [10.3847/2041-8213/ac772f](https://doi.org/10.3847/2041-8213/ac772f)
- Lafrenière, D., Jayawardhana, R., van Kerkwijk, M. H., Brandeker, A., & Janson, M. 2014, *ApJ*, 785, 47, doi: [10.1088/0004-637X/785/1/47](https://doi.org/10.1088/0004-637X/785/1/47)
- Lafrenière, D., Marois, C., Doyon, R., & Barman, T. 2009, *ApJ*, 694, L148, doi: [10.1088/0004-637X/694/2/L148](https://doi.org/10.1088/0004-637X/694/2/L148)
- Lafrenière, D., Marois, C., Doyon, R., Nadeau, D., & Artigau, É. 2007, *ApJ*, 660, 770, doi: [10.1086/513180](https://doi.org/10.1086/513180)
- Lagrange, A.-M., Bonnefoy, M., Chauvin, G., et al. 2010, *Sci*, 329, 57, doi: [10.1126/science.1187187](https://doi.org/10.1126/science.1187187)
- Lagrange, A. M., Meunier, N., Rubini, P., et al. 2019, *Nature Astronomy*, 3, 1135, doi: [10.1038/s41550-019-0857-1](https://doi.org/10.1038/s41550-019-0857-1)
- Langlois, M., Gratton, R., Lagrange, A.-M., et al. 2021, *A&A*, 651, A71, doi: [10.1051/0004-6361/202039753](https://doi.org/10.1051/0004-6361/202039753)
- Lee, J., & Song, I. 2019, *MNRAS*, doi: [10.1093/mnras/stz1044](https://doi.org/10.1093/mnras/stz1044)
- Li, Y., Brandt, T. D., Brandt, G. M., et al. 2023, *arXiv e-prints*, arXiv:2301.10420, doi: [10.48550/arXiv.2301.10420](https://doi.org/10.48550/arXiv.2301.10420)
- Liu, M. C., Dupuy, T. J., & Allers, K. N. 2016, *ApJ*, 833, 96, doi: [10.3847/1538-4357/833/1/96](https://doi.org/10.3847/1538-4357/833/1/96)
- Liu, M. C., Dupuy, T. J., & Leggett, S. K. 2010, *ApJ*, 722, 311, doi: [10.1088/0004-637X/722/1/311](https://doi.org/10.1088/0004-637X/722/1/311)
- Liu, M. C., Magnier, E. A., Deacon, N. R., et al. 2013, *ApJ*, 777, L20, doi: [10.1088/2041-8205/777/2/L20](https://doi.org/10.1088/2041-8205/777/2/L20)
- Lo Curto, G., Pepe, F., Avila, G., et al. 2015, *Msngr*, 162, 9
- Luck, R. E. 2018, *AJ*, 155, 111, doi: [10.3847/1538-3881/aaa9b5](https://doi.org/10.3847/1538-3881/aaa9b5)
- Lucy, L. B., & Sweeney, M. A. 1971, *AJ*, 76, 544, doi: [10.1086/111159](https://doi.org/10.1086/111159)
- Macintosh, B., Graham, J. R., Ingraham, P., et al. 2014, *PNAS*, 111, 12661, doi: [10.1073/pnas.1304215111](https://doi.org/10.1073/pnas.1304215111)
- Macintosh, B., Graham, J. R., Barman, T., et al. 2015, *Science*, 350, 64, doi: [10.1126/science.aac5891](https://doi.org/10.1126/science.aac5891)
- Maire, A.-L., Bonnefoy, M., Ginski, C., et al. 2016, *A&A*, 587, A56, doi: [10.1051/0004-6361/201526594](https://doi.org/10.1051/0004-6361/201526594)
- Marois, C., Lafrenière, D., Doyon, R., Macintosh, B., & Nadeau, D. 2006, *ApJ*, 641, 556, doi: [10.1086/500401](https://doi.org/10.1086/500401)
- Mayor, M., Pepe, F., Queloz, D., et al. 2003, *The Messenger*, 114, 20
- McKinney, W. 2010, in *Proceedings of the 9th Python in Science Conference*, Austin, Texas, 56–61, doi: [10.25080/Majora-92bf1922-00a](https://doi.org/10.25080/Majora-92bf1922-00a)
- Mesa, D., Gratton, R., Kervella, P., et al. 2023, *AF Lep b: The Lowest Mass Planet Detected Coupling Astrometric and Direct Imaging Data*, doi: [10.48550/arXiv.2302.06213](https://doi.org/10.48550/arXiv.2302.06213)
- Metchev, S. A., & Hillenbrand, L. A. 2009, *ApJS*, 181, 62, doi: [10.1088/0067-0049/181/1/62](https://doi.org/10.1088/0067-0049/181/1/62)
- Miret-Roig, N., Galli, P. A. B., Brandner, W., et al. 2020, *A&A*, 642, A179, doi: [10.1051/0004-6361/202038765](https://doi.org/10.1051/0004-6361/202038765)
- Mollière, P., & Mordasini, C. 2012, *A&A*, 547, A105, doi: [10.1051/0004-6361/201219844](https://doi.org/10.1051/0004-6361/201219844)
- Moór, A., Szabó, Gy. M., Kiss, L. L., et al. 2013, *MNRAS*, 435, 1376, doi: [10.1093/mnras/stt1381](https://doi.org/10.1093/mnras/stt1381)
- Moór, A., Pawellek, N., Ábrahám, P., et al. 2020, *AJ*, 159, 288, doi: [10.3847/1538-3881/ab8f98](https://doi.org/10.3847/1538-3881/ab8f98)
- Mugrauer, M., Röhl, T., Ginski, C., et al. 2012, *MNRAS*, 424, 1714, doi: [10.1111/j.1365-2966.2012.21216.x](https://doi.org/10.1111/j.1365-2966.2012.21216.x)
- Mugrauer, M., Vogt, N., Neuhauser, R., & Schmidt, T. O. B. 2010, *A&A*, 523, L1, doi: [10.1051/0004-6361/201015523](https://doi.org/10.1051/0004-6361/201015523)
- Musso Barucci, A., Cugno, G., Launhardt, R., et al. 2019, *A&A*, 631, A84, doi: [10.1051/0004-6361/201936510](https://doi.org/10.1051/0004-6361/201936510)
- Nielsen, E. L., De Rosa, R. J., Macintosh, B., et al. 2019, *AJ*, 158, 13, doi: [10.3847/1538-3881/ab16e9](https://doi.org/10.3847/1538-3881/ab16e9)
- Nowak, M., Lacour, S., Lagrange, A.-M., et al. 2020, *A&A*, 642, L2, doi: [10.1051/0004-6361/202039039](https://doi.org/10.1051/0004-6361/202039039)
- Pepe, F., Mayor, M., Rupprecht, G., et al. 2002, *The Messenger*, 110, 9

- Phillips, C. L., Bowler, B. P., Mace, G., Liu, M. C., & Sokal, K. 2020a, *ApJ*, 896, 173, doi: [10.3847/1538-4357/ab9111](https://doi.org/10.3847/1538-4357/ab9111)
- Phillips, M. W., Tremblin, P., Baraffe, I., et al. 2020b, *A&A*, 637, A38, doi: [10.1051/0004-6361/201937381](https://doi.org/10.1051/0004-6361/201937381)
- Plavchan, P., Barclay, T., Gagné, J., et al. 2020, *Nature*, 582, 497, doi: [10.1038/s41586-020-2400-z](https://doi.org/10.1038/s41586-020-2400-z)
- Reid, I. N., & Hawley, S. L. 2005, *New Light on Dark Stars : Red Dwarfs, Low-Mass Stars, Brown Dwarfs*, doi: [10.1007/3-540-27610-6](https://doi.org/10.1007/3-540-27610-6)
- Saumon, D., & Marley, M. S. 2008, *ApJ*, 689, 1327, doi: [10.1086/592734](https://doi.org/10.1086/592734)
- Schmidt, T. O. B., Mugrauer, M., Neuhäuser, R., et al. 2014, *A&A*, 566, A85, doi: [10.1051/0004-6361/201321625](https://doi.org/10.1051/0004-6361/201321625)
- Schneider, A. C., Windsor, J., Cushing, M. C., Kirkpatrick, J. D., & Shkolnik, E. L. 2017, *AJ*, 153, 196, doi: [10.3847/1538-3881/aa6624](https://doi.org/10.3847/1538-3881/aa6624)
- Scuflaire, R., Théado, S., Montalbán, J., et al. 2008, *Ap&SS*, 316, 83, doi: [10.1007/s10509-007-9650-1](https://doi.org/10.1007/s10509-007-9650-1)
- Sepulveda, A. G., & Bowler, B. P. 2022, *AJ*, 163, 52, doi: [10.3847/1538-3881/ac3bb5](https://doi.org/10.3847/1538-3881/ac3bb5)
- Service, M., Lu, J. R., Campbell, R., et al. 2016, *PASP*, 128, 095004, doi: [10.1088/1538-3873/128/967/095004](https://doi.org/10.1088/1538-3873/128/967/095004)
- Shkolnik, E. L., Allers, K. N., Kraus, A. L., Liu, M. C., & Flagg, L. 2017, *AJ*, 154, 69, doi: [10.3847/1538-3881/aa77fa](https://doi.org/10.3847/1538-3881/aa77fa)
- Spiegel, D. S., Burrows, A., & Milsom, J. A. 2011, *ApJ*, 727, 57, doi: [10.1088/0004-637X/727/1/57](https://doi.org/10.1088/0004-637X/727/1/57)
- Stolker, T., Quanz, S. P., Todorov, K. O., et al. 2020, *A&A*, 635, A182, doi: [10.1051/0004-6361/201937159](https://doi.org/10.1051/0004-6361/201937159)
- Tetzlaff, N., Neuhäuser, R., & Hohle, M. M. 2011, *MNRAS*, 410, 190, doi: [10.1111/j.1365-2966.2010.17434.x](https://doi.org/10.1111/j.1365-2966.2010.17434.x)
- Torres, C. A. O., Quast, G. R., da Silva, L., et al. 2006, *A&A*, 460, 695, doi: [10.1051/0004-6361:20065602](https://doi.org/10.1051/0004-6361:20065602)
- Trifonov, T., Tal-Or, L., Zechmeister, M., et al. 2020, *A&A*, 636, A74, doi: [10.1051/0004-6361/201936686](https://doi.org/10.1051/0004-6361/201936686)
- van Dokkum, P. G. 2001, *PASP*, 113, 1420, doi: [10.1086/323894](https://doi.org/10.1086/323894)
- Vigan, A., Fontanive, C., Meyer, M., et al. 2021, *A&A*, 651, A72, doi: [10.1051/0004-6361/202038107](https://doi.org/10.1051/0004-6361/202038107)
- Virtanen, P., Gommers, R., Oliphant, T. E., et al. 2020, *Nature Methods*, 17, 261, doi: [10.1038/s41592-019-0686-2](https://doi.org/10.1038/s41592-019-0686-2)
- Vousden, W. D., Farr, W. M., & Mandel, I. 2016, *MNRAS*, 455, 1919, doi: [10.1093/mnras/stv2422](https://doi.org/10.1093/mnras/stv2422)
- Wang, J. J., Ruffio, J.-B., Morris, E., et al. 2021, *AJ*, 162, 148, doi: [10.3847/1538-3881/ac1349](https://doi.org/10.3847/1538-3881/ac1349)
- Wizinowich, P. 2013, *PASP*, 125, 798, doi: [10.1086/671425](https://doi.org/10.1086/671425)
- Zúñiga-Fernández, S., Bayo, A., Elliott, P., et al. 2021, *A&A*, 645, A30, doi: [10.1051/0004-6361/202037830](https://doi.org/10.1051/0004-6361/202037830)
- Zuckerman, B., Rhee, J. H., Song, I., & Bessell, M. S. 2011, *ApJ*, 732, 61, doi: [10.1088/0004-637X/732/2/61](https://doi.org/10.1088/0004-637X/732/2/61)
- Zuckerman, B., Song, I., Bessell, M. S., & Webb, R. A. 2001, *ApJ*, 562, L87, doi: [10.1086/337968](https://doi.org/10.1086/337968)